IOP PUBLISHING PLASMA PHYSICS AND CONTROLLED FUSION

Plasma Phys. Control. Fusion **49** (2007) B173–B182 doi:10.1088/0741-3335/49/12B/S16

Global full-f gyrokinetic simulations of plasma turbulence

V Grandgirard[1], Y Sarazin[1], P Angelino[1], A Bottino[2], N Crouseilles[3], G Darmet[1], G Dif-Pradalier[1], X Garbet[1], Ph Ghendrih[1], S Jolliet[4], G Latu[5], E Sonnendrücker[3] and L Villard[4]

[1] CEA/DSM/DRFC, Association Euratom-CEA, Cadarache, 13108 St Paul-lez-Durance, France
[2] Max Plank Institut fr Plasmaphysik, IPP-EURATOM AssociationGarching, Germany
[3] IRMA, Université Louis Pasteur, 7, rue René Descartes, 67084 Strasbourg Cedex, France
[4] CRPP, Association Euratom-Confédération Suisse, EPFL, 1015 Lausanne, Switzerland
[5] LaBRI, 341 Cours Libération, 33405 Talence Cedex, France

E-mail: virginie.grandgirard@cea.fr

Received 6 July 2007
Published 15 November 2007
Online at stacks.iop.org/PPCF/49/B173

Abstract

Critical physical issues can be specifically tackled with the global full-f gyrokinetic code GYSELA. Three main results are presented. First, the self-consistent treatment of equilibrium and fluctuations highlights the competition between two compensation mechanisms for the curvature driven vertical charge separation, namely, parallel flow and polarization. The impact of the latter on the turbulent transport is discussed. In the non-linear regime, the benchmark with the Particle-In-Cell code ORB5 looks satisfactory. Second, the transport scaling with ρ_* is found to depend both on ρ_* itself and on the distance to the linear threshold. Finally, a statistical steady-state turbulent regime is achieved in a reduced version of GYSELA by prescribing a constant heat source.

(Some figures in this article are in colour only in the electronic version)

1. Introduction

Gyrokinetic codes are now mature enough to address experimentally relevant pieces of physics [1–4]. In this framework, global and full-f codes allow one to specifically address physical issues of outermost importance in fusion devices. Due to their huge demands in terms of both numerical memory and CPU time consumption, such full-f simulations have become possible only very recently. On the one hand, simulating a whole part of the tokamak cross-section allows one to capture large scale transport events, eventually leading to non-local transport and turbulence spreading. In particular, such processes can bring new ingredients into the physics governing scaling laws. On the other hand, full-f codes solve self-consistently solve the equilibrium and the fluctuations, without any scale separation assumption. In this case,

properly defining the gyrokinetic equilibrium is crucial to discriminate between instability driven fluctuations and time evolution towards the equilibrium. Besides, non-equilibrium initial states can also impact the turbulence dynamics itself. Finally, full-f codes open the route towards more realistic flux driven models, where the turbulence drive is no longer ensured by a prescribed gradient or fixed thermal baths at the boundaries, but by an incoming heat and/or particle source such as in the experiments.

This paper focuses on some of the physical implications of global and full-f gyrokinetic codes. The 5D GYSELA (GYrokinetic SEmi-LAgrangian) code is used to model the ion temperature gradient (ITG) driven turbulence with a semi-Lagrangian numerical scheme [5]. The model is detailed in section 2. The problem of solving the gyrokinetic equilibrium, especially in full-f codes such as Gysela, is addressed in section 3. As reported earlier [6], the code has already been benchmarked, both linearly and non-linearly against the CYCLONE test case [7]. In section 4, a further validation based on non-linear comparisons with the ORB5 code [8] is presented. Results on the ρ_* scaling of the turbulent transport, ρ_* being the ratio of the ion Larmor radius ρ_i to the minor radius a, are reported in section 5. Consistently with previous works, the correlation time and correlation length are found to be consistent with the gyroBohm, respectively Bohm, scaling at small ρ_* and above the linear threshold, respectively, at large ρ_* and close to the threshold. Finally, turbulence in the flux driven regime is investigated with a reduced 3D gyrokinetic model, used as a paradigm, section 6. The bursty character of the dynamics, as well as the departure from the Maxwellian, is reported.

2. Gyrokinetic system solved by GYSELA

The model focuses on the turbulent transport driven by the collisionless ITG driven instability in the electrostatic regime. The simplified geometry consists of concentric toroidal magnetic flux surfaces with circular poloidal cross-sections. The magnetic field is $\vec{B} = (B_0 R_0/R)(\vec{e}_\varphi + (r/qR_0)\vec{e}_\theta)$. B_0 and R_0 are the magnetic field and the major radius of the torus at the magnetic axis, with $R = R_0 + r\cos\theta$. $\vec{e}_\theta$ and $\vec{e}_\varphi$ are the unit vectors in the two periodic directions, poloidal and toroidal, respectively. The safety factor profile is $q(r) = 0.854 + 2.184(r/a)^2$. In the low frequency turbulence regime $\omega \ll \omega_c = e_\mathrm{i}B_0/m_\mathrm{i}$, the gyrokinetic description is appropriate. $v_\parallel$ is the velocity parallel to the magnetic field, and the magnetic moment $\mu = m_\mathrm{i}v_\perp^2/(2B)$ is an adiabatic invariant. GYSELA solves the time evolution of the 5D guiding-centre distribution function $\bar{f}(r, \theta, \varphi, v_\parallel, \mu, t)$:

$$\partial_t \bar{f} + (\vec{v}_E + \vec{v}_D)\cdot\vec{\nabla}_\perp \bar{f} + (v_\parallel/R)\partial_\varphi \bar{f} + \dot{v}_\parallel \partial_{v_\parallel} \bar{f} = 0 \tag{1}$$

with $\vec{\nabla}_\perp = (\partial_r, 1/r\partial_\theta)$. $\vec{v}_{\bar{E}} = \vec{B}\times\vec{\nabla}(\mathcal{J}.\phi)/B^2$ is the electric drift velocity and ϕ the electric potential. The gyroaverage operator $\mathcal{J}$ corresponds to the zero order Bessel function $J_0(k_\perp\rho_\mathrm{i})$ in Fourier space, ρ_i being the ion Larmor radius. It is replaced by a Padé approximation in the code [9]. At low β, the curvature drift velocity is equal to $\vec{v}_D = ((m_\mathrm{i}v_\parallel^2 + \mu B)/eB^3)\vec{B}\times\vec{\nabla}B$. In the large aspect ratio limit, $m_\mathrm{i}\dot{v}_\parallel = e_\mathrm{i}E_\parallel - \mu\nabla_\parallel B + mv_\parallel\vec{v}_E\cdot\vec{\nabla}B/B$ with $\nabla_\parallel = 1/R[\partial_\varphi + (1/q(r))\partial_\theta]$. The self-consistency is ensured by the quasi-neutrality constraint, the electrons being assumed adiabatic:

$$-\frac{1}{n_0(r)}\nabla_\perp\cdot\left[\frac{n_0(r)}{B_0\omega_c}\nabla_\perp\phi\right] + \frac{e}{T_\mathrm{e}(r)}[\phi - \langle\phi\rangle] = \frac{1}{n_0(r)}[n_\mathrm{Gi}(r,\theta,\varphi) - n_{\mathrm{Gi}_\mathrm{init}}(r,\theta)]. \tag{2}$$

The polarization term (first term on the left-hand side) accounts for the difference between the ion guiding-centre density $n_\mathrm{Gi} = 2\pi B(r,\theta)/m_\mathrm{i}\int \mathrm{d}\mu\int \mathrm{d}v_\parallel \mathcal{J}.\bar{f}$ and the particle density. The brackets $\langle\cdot\rangle$ refer to the flux surface average $\langle\cdot\rangle = 1/(2\pi)^2\int\int\cdot\,\mathrm{d}\theta\,\mathrm{d}\phi$. The correction term

$n_{\mathrm{Gi}_{\mathrm{init}}}$ is equal to $n_{\mathrm{Gi}_{\mathrm{init}}} = 2\pi B(r,\theta)/m_{\mathrm{i}} \int \mathrm{d}\mu \int \mathrm{d}v_{\parallel} \mathcal{J}.f_{\mathrm{init}}$, f_{init} being the initial distribution function. More details on the system are given in [6].

Since the electrons are adiabatic, there is no net particle transport. Hence, the radial density profile remains constant in time. f is a prescribed Maxwellian at both radial boundaries, with two different temperatures. f_{init} is either a local Maxwellian or a canonical Maxwellian, as discussed in section 3. Perturbations are added as a sum of (m,n) Fourier modes with random phase and small magnitude. m and n are the poloidal and toroidal wave numbers, respectively. The quasi-neutrality equation (2) is solved in Fourier space for the poloidal and toroidal directions, while finite differences are used in the radial direction. The gyrokinetic equation (1) is solved with a semi-Lagrangian scheme [10], which has already proven to be powerful in a reduced 4D version of the code, focusing on the slab branch of the ITG turbulence in the drift-kinetic limit [5]. Significant effort has been devoted to improving the code parallelization [11,12], which is especially difficult for Eulerian-like numerical schemes. The present version exhibits an efficacity of about 70% on 1024 processors.

3. Non-linear simulations with a global full-f code

Several publications [13, 14] have stressed the importance of initializing gyrokinetic simulations with a well-defined equilibrium. In the absence of collisions, an equilibrium distribution function fulfils $[H_{\mathrm{eq}}, f_{\mathrm{eq}}] = 0$, with $[.,.]$ the Poisson bracket. The equilibrium gyrokinetic Hamiltonian H_{eq} depends on the motion invariants only, namely, the energy $\mathcal{E}$, the magnetic moment μ and the toroidal momentum P_{φ}. Consequently, any function of $\mathcal{E}$, μ and P_{φ} will satisfy the equilibrium conditions. A convenient form is provided by a local Maxwellian where the radius is replaced by an effective radial coordinate $\bar{r}$ function of the invariants [15,16]. This corresponds to the so-called *canonical Maxwellian* initialization f_{CM}. In such an equilibrium, the curvature drift which induces a vertical charge polarization is compensated by the ion parallel flow. This flow, analogous to the Pfirsch–Schlüter current carried by the electrons, naturally emerges from the $v_{\parallel}$ dependence of P_{φ}. Indeed, the distribution function f_{CM} is *not even in* $v_{\parallel}$ unlike the local Maxwellian f_{LM}. f_{LM} does not carry any parallel flow and the charge separation gives rise to a large scale electric field. In this case, the charge separation tends to be compensated by the polarization flow. The early dynamics of the resulting electric potential ϕ can be predicted analytically, as will be detailed in a forthcoming publication. At leading order, it is governed by the curvature drift. In particular, it is found that $\phi \approx \phi_{00} + \phi^s_{10} \sin\theta + \phi^c_{10} \cos\theta$, with $e\phi_{00}/T_0 \propto \rho_*^2(\omega_c t)^2$ and $e\phi^s_{10}/T_0 \propto \rho_*^2 \omega_c t$, consistently with the numerical simulations. Such a ρ_*^2 dependence does not mean that these flows remain weak at small ρ_*. Indeed, an upper boundary of the time duration of the growth of these flows is given by the time at which the parallel dynamics counterbalances the charge polarization. In the end, the saturation level of these flows is significant and of the order of a few tenths of T_0/e. Conversely, the cosine component ϕ^c_{10} is orders of magnitude smaller. The $\sin\theta$ component ϕ^s_{10} grows first, linearly in time, as a result of the up–down asymmetry of the curvature drift. The oscillatory behaviour at the geodesic acoustic mode (GAM) frequency is recovered at later times, when the $E \times B$ drift is no longer negligible and enters the dynamics.

An interesting question is whether such sheared flows, which result from the re-arrangement of non-equilibrium initialization, can durably prevent the onset of turbulence. Two simulations at $\rho_* = 5 \times 10^{-3}$ and with the same initial temperature gradient—well above the threshold—are compared. They only differ by their initial distribution function, either canonical or Maxwellian. The time evolution of the heat diffusivity is plotted in figure 1. The turbulent transport is clearly delayed when starting from an initial local Maxwellian, by about $1\,500\,\omega_c^{-1}$ in this case. As seen in the inset, the effective growth rate is reduced for the local

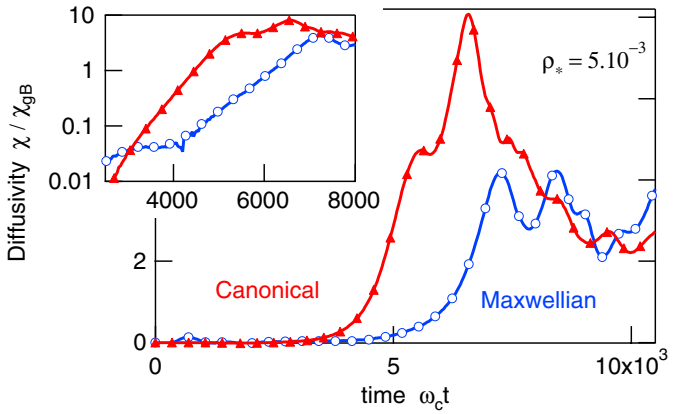

Figure 1. Time evolution of the turbulent transverse diffusivity $\chi_\perp$ ($\rho_* = 1/200$) when initializing the distribution function with a canonical equilibrium or a local Maxwellian. Top panel: zoom in log-lin scale.

Maxwellian (from $\gamma_{\rm CM} \approx 2.3\,10^{-3}\omega_c$ to $\gamma_{\rm LM} \approx 1.5\,10^{-3}\omega_c$), when sheared flows are present. Such a picture qualitatively agrees with a reduction of the effective linear growth rate by the shearing rate. Also, the turbulence overshoot at the end of the linear phase is smeared out. However, both simulations yield similar diffusivities in the turbulent regime, as exemplified by the values at the end of the simulations, see figure 1.

4. Non-linear benchmarks with ORB5 code

The GYSELA code has been benchmarked against the CYCLONE test case [7], both linearly and non-linearly, as reported earlier [6]. Also, the now standard test of poloidal flow screening in the collisionless regime [17] has been performed successfully. Here, we report first results of the non-linear comparison with the ORB5 code [8]. Both codes are global and model the same gyrokinetic equations. However, ORB5 uses a completely different numerical scheme. It is a δf Particle-in-Cell (PIC) code. Here, the perturbed part of the distribution function $\delta f = f - f_{\rm init}$ is sampled by a random distribution of markers, according to the Monte Carlo method. The positions of the markers are evolved in time following the characteristics of the gyrokinetic equation (Lagrangian method). The time evolution uses a 4th order Runge–Kutta scheme and the quasi-neutrality equation is solved with a 3D finite element method. The gyroaverage is approximated by an adaptive numerical average. Another difference resides in the zonal flow term $\bar{\phi}$ which is approximated by ϕ_{00} in GYSELA, while the full geometric coupling is kept in ORB5. Finally, the right-hand side of the quasi-neutrality equation is Fourier-filtered along the magnetic field lines ($m = nq(s) \pm \Delta m$) in ORB5. This leads to a reduction of the statistical noise associated with the PIC discretization by filtering out the non-physical high $k_\parallel$ modes [18].

The parameters for the benchmark are based on the CYCLONE test case [7]. The minor radius is $a = 0.625$ m, the inverse aspect ratio $\varepsilon = a/R = 0.36$ and the magnetic field on axis $B_0 = 1.91$ T. The initial temperature gradients are given by $\mathrm{d}\log T/\mathrm{d}r = -L_T^{-1}[-1+\cosh^{-2}((r-0.1a)/0.04)+\cosh^{-2}((r-0.9a)/0.04)]$ with the conditions $T_{\rm e}(r/a = 0.5) = T_{\rm i}(r/a = 0.5) = 2$ KeV. The ratio of the temperature gradient length over the density one is $L_T/L_n = 0.21$. Notice that the mean temperature profile is not frozen. As a result of

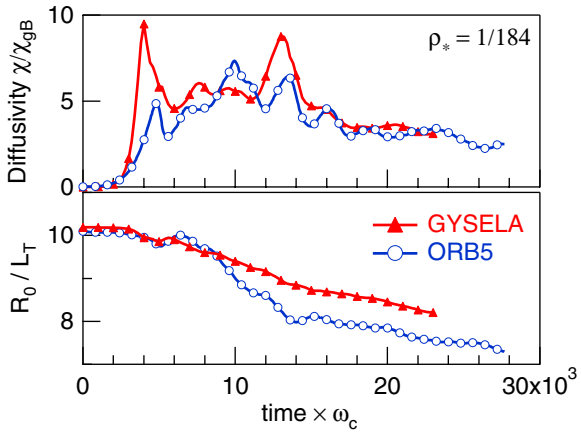

Figure 2. Time evolutions of the turbulent transverse diffusivity $\chi_\perp$ (top) and of the normalized temperature gradient (bottom) in GYSELA and ORB5 for $\rho_* = 1/184.7$.

the turbulent heat flux, the temperature gradient decreases with time. The boundary conditions are somewhat different in both codes: while the temperature is kept constant at both radial boundaries in GYSELA, leading to steep gradients within thin boundary layers, the core boundary temperature is free to evolve in ORB5, leading to a decaying turbulence regime.

The two simulations are at $\rho_* = 1/184.7$. GYSELA uses about 1 billion grid points in the 5D phase space, while ORB5 uses about 33 millions of grid points in space with 256 millions of pseudo-particles. Both simulations ran roughly 36 hours on 128 processors, using machines of similar performances. The time evolutions of the transverse diffusivity $\chi_\perp$, normalized to the gyroBohm diffusivity $\chi_{gB} = \rho_s^2 c_s / L_n$ (c_s is the sound speed), and of the normalized temperature gradient R_0/L_T are plotted in figure 2. Both quantities are averaged over flux surfaces, as well as over the radial interval $0.4 \leqslant r/a \leqslant 0.6$. The time is shifted by about $-7.10^3 \omega_c^{-1}$ for the ORB5 simulation so as to account for the longer transient at the beginning of this code. First, one observes that GYSELA and ORB5 yield the same level of turbulent transport in the non-linear regime. Also, such magnitudes of $\chi_\perp$ are in agreement with those reported in other gyrokinetic simulations [7]. Second, the temperature profile relaxes faster in ORB5 than in GYSELA. Such a difference could result from the difference in the boundary conditions: while the whole profile freely evolves in ORB5, the temperature is kept constant at the radial boundaries in GYSELA. Also note that, at a given value of R_0/L_T, ORB5 predicts a larger transport than GYSELA. Such a mismatch could result from the intrinsic difference between full-f and δf schemes. Indeed, the equilibrium electric field is self-consistently computed in GYSELA (cf section 3). This likely leads to a larger magnitude of the zonal component ϕ_{00} and of the resulting poloidal velocity shear in GYSELA, possibly reducing the turbulent transport level. This benchmark will be further detailed in a future publication.

5. Transport scaling with ρ_*

The kinetic equation exhibits scale invariance properties [19]. As a consequence, the energy confinement time τ_E is expected to be governed by a set of key dimensionless parameters. A key quantity is the ρ_* parameter, since the present devices cannot access the small ρ_* values

expected in ITER, of the order of 2×10^{-3}. In the JET tokamak, the most performing discharges have 2–3 times larger ρ_*. Furthermore, in the empirical scaling laws of τ_E, the power exponent of ρ_* is the largest, namely, $\omega_c\tau_E \propto \rho_*^{-2.8}$. Such a power law is consistent with the so-called gyroBohm scaling ($\chi_\perp \approx \rho_*\chi_\mathrm{B}$ and $\chi_\mathrm{B} = \rho_i^2\omega_c$), so that $\omega_c\tau_E \approx \omega_c a^2/\chi_\perp \propto \rho_*^{-3}$. After the pioneering works used fluid models to investigate this critical issue [20], two recent gyro-kinetic simulations [1, 21] report a transition from Bohm to gyroBohm scaling when ρ_* decreases towards ITER-like values. Two open issues remain: what is the ρ_* value of this transition? What is the physical mechanism? So far, two main explanations have been proposed. On the one hand, shear flow stabilization leads to $\chi_\perp \approx \rho_*\chi_\mathrm{B}(1-\alpha\rho_*)$ [22]. This results from the scaling of the $E\times B$ shearing rate like $\gamma_E \approx \rho_*\gamma_\mathrm{lin}$, with $\gamma_\mathrm{lin} \approx (k_\theta\rho_\mathrm{i})\,c_\mathrm{s}/(RL_T)^{1/2}$ the linear growth rate of the instability in the absence of shear flow. On the other hand, large scale transport events can lead to large correlation lengths of the form $\lambda_c \approx (a\rho_\mathrm{i})^{1/2}$. In this case, non-diffusive transport or turbulence spreading is expected to be at work. The latter mechanism leads to the same type of scaling for the diffusivity at small ρ_*, namely, $\chi_\perp \approx \rho_*\chi_\mathrm{B}/(1+\alpha\rho_*)$ [23]. Such physics can only be addressed with global codes.

A ρ_* scan has been performed with GYSELA to study this question. Three values have been analysed, ranging from large ($\rho_* = 2\times10^{-2}$) to intermediate ($\rho_* = 10^{-2}$ and $\rho_* = 5\times10^{-3}$) values. Since the equilibrium is allowed to evolve in GYSELA, the mean temperature profile tends to relax towards the threshold (at $R/L_T \approx 6$) in the turbulent regime. Such dynamics are apparent in figure 3. The dotted line refers to the best fit of the Lawrence Livermore National Laboratory results (flux-tube PIC code) for the CYCLONE case [7]. Also, the three cases do not start from the same temperature gradient. This results from the difficulty in matching radial profiles at different ρ_*, when initializing with a canonical distribution function [15] (see section 3). The correlation length and time of the electric potential fluctuations are presented in figures 4 and 5 for two different choices of t_0: either when the system is still well above the threshold (figures 4(*a*) and (*b*)), i.e. rather early in the simulation, or close to the threshold (figures 5(*a*) and (*b*)), at the end of the simulation. For both values of t_0, the three curves are not far from overlapping with the time lag Δt normalized to a/c_s. This suggests a rather weak dependence on ρ_* of the correlation time, whatever the departure from the threshold and the magnitude of ρ_*. This scaling is expected when the correlation time scales like $\tau_c \approx a/c_\mathrm{s}$. This is the case when the correlation is governed either by the parallel dynamics ($\tau_c \approx qR/v_\parallel \approx a/c_\mathrm{s}$ at fixed aspect ratio R/a) or by the turbulence broadening ($\tau_c \approx \Delta\omega^{-1} \approx \omega_*^{-1} \propto a/c_\mathrm{s}$ at $k_\theta\rho_\mathrm{i} = \mathrm{const}$). The small mismatches observed in figure 4(*a*) for the case $\rho_* = 5\times10^{-3}$ suggest that the correlation time weakly departs from this scaling at small ρ_* and far from the threshold. Since the correlation time seems to roughly scale like $\tau_c \approx a/c_\mathrm{s}$, the Bohm or gyroBohm scalings would correspond to correlation lengths of the order $\lambda_c \approx (a\rho_\mathrm{i})^{1/2}$ or $\lambda_c \approx \rho_\mathrm{i}$, respectively. Such scalings are systematically checked for the two sets of analyses, above (figure 4(*b*)) and close to (figure 5(*b*)) the threshold. The conclusions are that λ_c seems to scale like the ion Larmor radius ρ_i at small ρ_* and above the threshold and like $(a\rho_\mathrm{i})^{1/2}$ at large ρ_* and close to the threshold. Bohm scaling is expected close to the threshold, due to possible long-lived structures reminiscent of linear global modes.

In summary, the ρ_* scaling appears to depend on both the distance to the threshold and on ρ_*: our results are consistent with Bohm-like scaling close to the threshold and for large ρ_*, while gyroBohm scaling seems to prevail above the threshold at small ρ_*. These results are consistent with previous publications. They put forward the need to go towards flux driven simulations, so as to reach a statistical steady-state with a well-defined mean temperature profile.

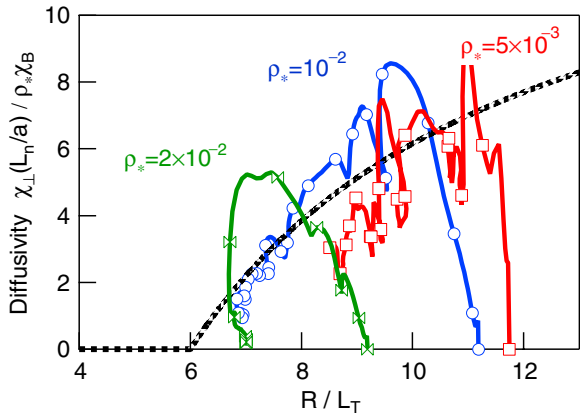

Figure 3. The time history of the system in the plane $(\chi_\perp; R/L_T)$ for three values of ρ_*. In each ρ_* case, the initial state lies on the horizontal axis. Dotted line: best fit of the LLNL results for CYCLONE [7].

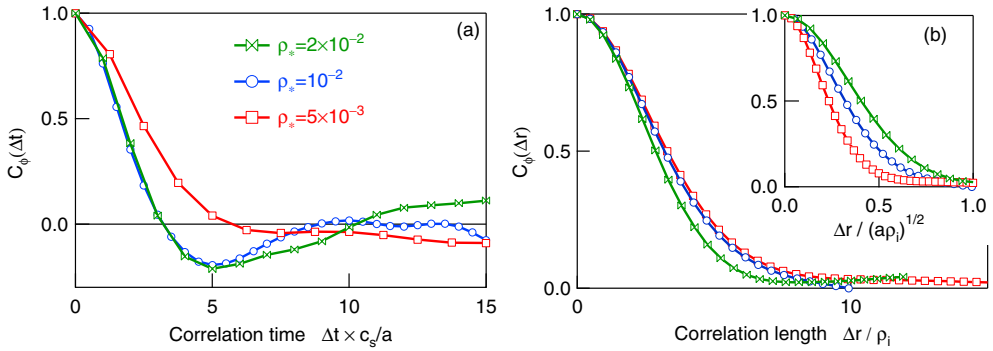

Figure 4. (*a*) Temporal self-correlation function $C_{\delta\phi}(\Delta t)$ and (*b*) radial self-correlation function $C_{\delta\phi}(\Delta r)$, for three values of ρ_*, well above the threshold.

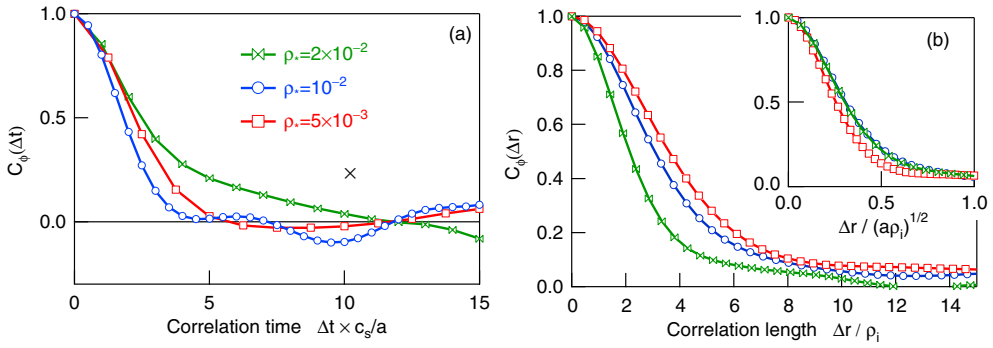

Figure 5. (*a*) Temporal self-correlation function $C_{\delta\phi}(\Delta t)$ and (*b*) radial self-correlation function $C_{\delta\phi}(\Delta r)$, for three values of ρ_*, close to the threshold.

6. Flux driven gyrokinetics

Most present gyrokinetic simulations set the system out of equilibrium by imposing two thermal baths as radial boundary conditions. As shown here, such a system then evolves leading to the relaxation of the gradients in the area of interest of the simulation domain. This evolution stops as the turbulence approaches the threshold where transport becomes very weak. In practice, during such a relaxation time, limited statistics are available to investigate the physics of scaling laws. An alternative approach is to maintain the system at prescribed gradients by prescribing ad hoc sources to maintain them. In the latter case, it is an issue to determine the impact of such a fluctuating source on the turbulent transport properties. As achieved in standard fluid codes, a more physical drive can be obtained by prescribing a source term in the system that imposes a given flux and analyzes the gradients as the response of flux driven turbulent transport. However, when going to gyrokinetic simulations this one-to-one relationship between a flux and a gradient is not as straightforward. Indeed, the gradients that are measured, say the temperature gradient, stem from a moment of the distribution function while the source term must be defined for each velocity of the distribution function and can thus generate gradients of higher moments of the distribution function.

First calculations of gyrokinetic flux driven systems [24] have been performed with a reduced gyrokinetic model that has been derived for deeply trapped ion turbulence [9, 25]. This system is 3D with two dimensions in real space, namely, a radial coordinate and an angle, and 1D in velocity space, the chosen coordinate being the energy. In such a system the source term is implemented at a small radius (core heat source) in the vicinity of the core boundary layer where a vanishing gradient of the distribution function is imposed (symmetry conditions). To satisfy the boundary conditions a buffer zone with strong radial diffusion is imposed. In the simulations reported here, the source term is located at the boundary of the core buffer zone. Statistical equilibrium of such a system will of course not be satisfied unless one imposes a sink, typically at the radial edge boundary. We have chosen a prescribed temperature at this boundary condition, namely the distribution function is constrained to be a Maxwellian at a fixed temperature $T_{\rm edge}$. The large radial diffusion coefficient in the edge buffer region then allows the imposed heat flux to be transported through this boundary.

The choice of the source term must be as generic as possible, and with respect to our present scope, steady-state. In the present versions of our gyrokinetic codes, adiabatic electrons prevent particle transport so that the source term must not be a particle source. A simple approach has been followed by introducing the basis of Laguerre polynomials $L_n(E)$, where E is the energy normalized to $T_{\rm edge}$ and n the order of the polynomial (the exponent of the largest power in E). These Laguerre functions form an orthogonal basis where the scalar product is the integral over the energy E weighted by the Maxwellian $\exp(-E)$, see [9]. In such a framework, the projection of the distribution function on the Laguerre polynomials, $G_k = \langle f|L_k\rangle$ (here $\langle f|g\rangle$ is the scalar product of f and g), is directly related to the fluid moments where the density is the projection on the zeroth order polynomial $L_0 = 1$ and the temperature $\sqrt{3/2}(T - T_{\rm edge})/T_{\rm edge}$ to the projection on $L_1 = \sqrt{2/3}(E - 3/2)$. For this reason the source term that has been used is $S = S_0(\psi)\, L_1(E)\, \exp(-E)$, where $S_0(\psi)$ stands for the radial localization labelled by ψ. By definition of such a source term, it only contributes to building up the moment $G_1 = \langle f|L_1\rangle$ and thus governs an increase in the temperature at the source location. However, via the transport properties of the reduced Vlasov equation, such a moment is coupled to all the other moments [9]. The transport problem at hand is therefore the generation by the source of all G_k moments—but G_0—towards the sink at the edge boundary, where all moments G_k are vanishing—but for $k = 0$. In practice, one finds that the time averaged moments (averaging over several confinement times) exhibit a flat profile between the very core and the source

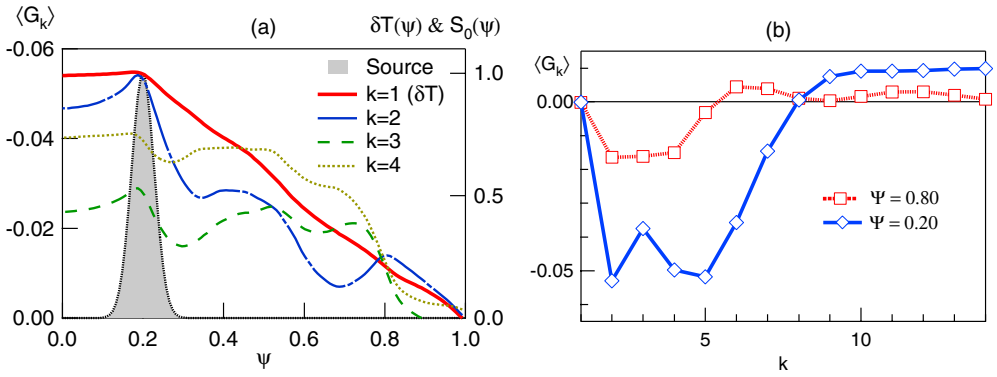

Figure 6. (*a*) Time average of the radial profiles of $\langle G_k \rangle$ ($1 \leqslant k \leqslant 4$) and the source term $S_0(\psi)$; (*b*) magnitude of $\langle G_k \rangle$ ($1 \leqslant k \leqslant 14$) at two different radial locations.

and a smooth gradient from the source towards the vanishing values at the edge, figure 6(*a*). Furthermore, one finds that the moment which exhibits the largest magnitude is the temperature moment, $k = 1$, figure 6(*b*). The higher order moments with $k = 2$ to $k = 5$ are one order of magnitude smaller. The even higher moments $k > 5$ are negligible. Unlike the thermal bath boundary condition [9], one finds that a limited number of moments are active in the system with a possible truncation of the moment series at $k = 5$. However, such a property is related to the specific kinetic properties that have been selected for the source and sink. In particular, a less constrained sink allowing for a departure from a Maxwellian distribution function would modify the kinetic distortion of the distribution function. A final remark is related to the time averaged profiles that all appear to fit a diffusive transport process although the evolution of the system is characterized by strong relaxation events and the interaction between large $E \times B$ convection cells (extending over a significant fraction of the radial box size) and zonal flows [24].

7. Conclusion

Global and full-f 5D gyrokinetic codes are able to address additional pieces of crucial physics. Since they are facing new challenges in terms of numerical resources, they have only started being developed rather recently. The GYSELA code is one of those. The semi-Lagrangian numerical scheme, as well as an efficient parallelization, allows it to capture the dynamics of the whole ion distribution function in a simplified toroidal geometry. This paper reports the satisfactory benchmark against the ORB5 code, modeling the same standard gyrokinetic equations for the ITG driven turbulence with a completely different numerical scheme. Three main physical issues have been discussed. First, the absence of scale separation assumption between equilibrium and fluctuations requires the former to be evaluated accurately. If not, large scale sheared flows are shown to develop so as to counterbalance the curvature driven vertical charge polarization. Such sheared flows are observed to reduce the effective linear growth rate as well as delay the onset of turbulence. Second, the scaling with ρ_* of the turbulent transport is investigated in a global geometry. Consistently with previous publications, the turbulence correlation properties are found to depend on ρ_* itself and on the distance to the threshold. The scaling looks like gyroBohm well above the threshold at small values of ρ_*. Third, flux driven conditions can be addressed in such full-f codes, leading to statistical steady-state turbulent regimes. In this case, special emphasis is laid on the departure of the

distribution function from the Maxwellian in a reduced 3D model for interchange-like turbulence. It will be especially interesting to investigate how such complex kinetic characteristics extrapolate to the more realistic 5D ITG turbulent regime.

Acknowledgments

The authors wish to acknowledge the constant support of C Passeron in the numerical development of the code. The strong commitment of M Boulet (CEA/DAM), who has performed several runs on the Tera10 super-computer within the 'Grand Challenge' project, is also warmly acknowledged.

References

[1] Waltz R, Candy J and Rosenbluth M 2002 *Phys. Plasmas* **9** 1938
[2] Lin Z, Chen L and Zonca F 2005 *Phys. Plasmas* **12** 056125
[3] Jenko F *et al* 2000 *Phys. Plasmas* **7** 1904
[4] Angelino P *et al* 2006 *Plasma Phys. Control. Fusion* **48** 557
[5] Grandgirard V *et al* 2006 *J. Comput. Phys.* **217** 395
[6] Grandgirard V *et al* 2008 *Commun. Nonlin. Sci. Numer. Simul.* **13** 81–7
[7] Dimits A M *et al* 2000 *Phys. Plasmas* **7** 969
[8] Bottino A *et al* 2001 *Proc. Int. Workshop on Theory of Fusion Plasma (Varenna, 2000)* p 327
[9] Sarazin Y *et al* 2005 *Plasma Phys. Control. Fusion* **47** 1817
[10] Sonnendrücker E and Roche J 1999 *J. Comput. Phys.* **149** 201
[11] Crouseilles N, Latu G and Sonnendrücker E 2006 Hermite splines interpolation on patches for a parallel solving of the Vlasov–Poisson equation *INRIA Report* RR5926
[12] Latu G, Crouseilles N, Grandgirard V and Sonnendrücker E 2007 Gyrokinetic semi-Lagrangian parallel simulation using a hybrid openMP/MPI programming *Recent Advances in Parallel Virtual Machine and Message Passing* (*Lecture Notes in Computer Science* vol 4757) (Berlin/Heidelberg: Springer) pp 356–64
[13] Idomura Y, Tokuda S and Kishimoto Y 2003 *Nucl. Fusion* **43** 234
[14] Angelino P *et al* 2006 *Phys. Plasmas* **13** 052304
[15] Dif-Pradalier G *et al* 2008 *Commun. Nonlin. Sci. Numer. Simul.* **13** 65–71
[16] Garbet X *et al* 2007 *Nucl. Fusion* **47** 1206
[17] Rosenbluth M N and Hinton F L 1998 *Phys. Rev. Lett.* **80** 724
[18] Jolliet S *et al* 2007 *Comput. Phys. Commun.* **177** 409
[19] Kadomtsev B B 1975 *Fiz. Plazmy* **1** 531
Kadomtsev B B 1975 *Sov. J. Plasma Phys.* **1** 295
[20] Ottaviani M *et al* 1997 *Phys. Rep.* **283** 121
[21] Lin Z *et al* 2002 *Phys. Rev. Lett.* **88** 195004
[22] Garbet G and Waltz R 1996 *Phys. Plasmas* **3** 1898
[23] Hahm T S *et al* 2004 *Plasma Phys. Control. Fusion* **46** A323
[24] Darmet G *et al* 2008 *Commun. Nonlin. Sci. Numer. Simul.* **13** 53–8
[25] Depret G *et al* 2000 *Plasma Phys. Control. Fusion* **42** 949